

Diabetic Retinopathy Detection using Geometrical Techniques related to the underlying Physiology

C.E. Hann¹, M. Narbot¹, M. MacAskill²

¹ Electrical & Computer Engineering, University of Canterbury, New Zealand.

² Van der Veer Institute and Department of Medicine, University of Otago, Christchurch, New Zealand.

Email: Chris.Hann@canterbury.ac.nz

Abstract

A computer algorithm is developed using a set of geometrical measures of Diabetic Retinopathy on fundus images. The algorithm is extended from previous work with a focus on accurately ruling out false exudates that are calculated from an initial screening. Sensitivities and specificities are used to measure the effectiveness of maintaining accurate detection of exudates while avoiding false positives with respect to an initial set of possible exudates. A very high specificity of 98.4% and good sensitivity of 88.6% on 12 images shows the potential of the method. These results justify future clinical trials involving Ophthalmologists. An eye tracking procedure that could characterize what regions of the retina that experienced Ophthalmologists focus on is discussed.

Keywords: Diabetic Retinopathy, Computer Algorithm, Physiology, Screening, Eye Tracking

1 Introduction

Diabetic retinopathy (DR) is retinopathy (damage to the retina) caused by complications of diabetes mellitus, which can eventually lead to blindness. DR is one of the main causes of blindness and visual impairment in developed countries [1,2]. It occurs when diabetes damages the tiny blood vessels inside the retina, the light-sensitive tissue at the back of the eye.

A healthy retina is necessary for good vision. Research indicates that at least 90% of these new cases could be reduced if there was proper and vigilant treatment and monitoring of the eyes [3]. In the United States the prevalence rates of retinopathy and vision threatening retinopathy are estimated to be 40.3 and 8.2%, respectively, for diabetic adults 40 years or older [4]. Diabetic retinopathy is the most frequent cause of new cases of blindness among adults aged 20–74 years.

During the first two decades of disease, nearly all patients with type 1 diabetes and >60% of patients with type 2 diabetes have retinopathy [5]. DR is the manifestation of systemic disease which affects up to 80% of all patients who have had diabetes for 10 years or more [6]. Within the next 15 to 30 years the number of people with diabetes is expected to double due to factors such as obesity, an aging population, and inactive lifestyles [7]. The high prevalence of diabetes therefore makes screening an expensive and time-consuming process.

The goal of a screening system is to detect the non proliferative stage of DR so that the disease can be managed appropriately to decrease the chances of vision impairment. DR grading using fundus images is significantly more sensitive than standard ophthalmoscopy, which can miss approximately 50% of subject with only micro aneurysms. Research has shown some potential for combining fundus photography and computer algorithms to automatically grade DR (e.g., see Abramoff and colleagues [8]). These algorithms search for bad lesions in the fundus images, which define the severity of DR. The lesions are categorized into microaneurysms, haemorrhages, and exudates based on their location, morphology, and color. However, the major problem with current computer algorithms is that to get high sensitivities, dramatically increases the number of false positives, which would make any wide spread screening method ineffective. The study of [8] shows that existing computer algorithms cannot yet be recommended for clinical practice.

This research takes an analytical approach to the diagnosis by using physiological information and geometry to characterize DR. Previous work [9] has developed techniques to detect the presence of DR with very high sensitivity and specificity of 96% and 97% respectively. A key part of the algorithm was using the property that contours of the R/G surface surrounding exudates and dot hemorrhages form tight closed curves.

The focus of the paper [9] was on proving the concept for potential screening. This paper significantly

extends the geometrical techniques of [9] and concentrates on accurate detection of the degree of DR rather than the presence or absence. The methods are tested on a number of images with a focus on exudates. The main result is a set of analytical, geometric tools that will form the basis for detecting any form of DR in future work. Finally, a discussion is presented on the potential use of eye tracking of ophthalmologists to characterize and put their “experience” into the computer algorithms. This initiative has possibilities of improving current algorithms and longer term maybe helping to train future ophthalmologists.

2 Methodology

All methods are developed with exudates as the case example, but could be equally applied to dot hemorrhages and other forms DR. The main purpose is to develop a set of mathematical tools that can describe the major physiological features of DR.

2.1 Initial screening method

The starting point of the algorithms is with a set of possible exudates which are found by a initial screening based on median filtering [9]. Quite low thresholds are used to ensure every true exudate is detected. The remaining false positives are then ruled out by a set of geometric measures. A summary of this method is given below, for more details and results see [9].

I. Define Optic Disk:

- Obtain top 0.5% of pixel intensities in green channel
- Place a rectangle around the largest connected region
- Define a circle with the centre at the left edge mid-point and radius of the horizontal width respectively
- Increase radius 50% to guarantee disk is bounded

II. Find Exudates Using Median Filter:

- Compute 50 pixel median filter along all vertical and horizontal lines. Median filter takes the moving median intensity value over 50 pixels (centered).
- Subtract the minimum of the median in each direction. From each pixel intensity to equalize the contrast over the image.

- For each vertical and horizontal line, select pixels with filtered intensities > 10 and take the union. If the filtered intensities > 30 and the green intensity > 100 , label the pixel I_{CE} , where CE= “confirmed exudate”.
- Form connected regions, remove regions with number of pixels < 5 . Remove regions containing pixels with red + green + blue channel < 60 , remove regions containing pixels in optic disc.

III. Add Pixels and Confirm Bright Exudates

- For each exudate compute the lower 5th percentile I_{low} and upper 95th percentile I_{high} of red/green (R/G) intensities. Within a ± 100 pixel neighbourhood of the exudate, select pixels where: $(R/G) \in [I_{low}, I_{high}]$. Add the selected pixels to the potential exudate if they are connected to the exudate.
- Save all connected regions that have pixels labelled I_{CE} . Remove these regions from the image analysis as they are confirmed as exudates.

IV. Set up contours for remaining exudates:

- In a 40-pixel neighbourhood of each remaining potential exudate, compute the R/G contours in steps of 0.05 ± 0.5 around the mean R/G for the exudate.
- Let $r_{EXUDATE}$ denote the radius of the unique circle, C , that precisely surrounds the exudate. Select a contour if:
 - a) Any part of contour is within $1.5 * r_{EXUDATE}$ from the centre of the circle
 - b) The contour has a length > 20 pixels
- For each selected contour, C , calculate the mean absolute gradient of the surrounding points and choose the contours corresponding to 7 largest values. If there are less than 7 contours select all the contours.

2.2 Geometric measures

2.2.1 Area and F_s

The algorithm chooses a minimum resolution for detecting exudates. This resolution is determined by first defining the area of a potential exudate:

$$area = \# pixels - boundary length \quad (1)$$

An area threshold of 6 is used to find potential exudates. The geometry of exudates is assumed to be close to a circle. Therefore a shape factor F_s defined:

$$F_s = \frac{A}{L_{max}^2} \quad (2)$$

where A is the area of the shape and L_{max} is the maximum distance between two pixels in the labeled region. Figure 1 shows three examples of the metric of Equation (2).

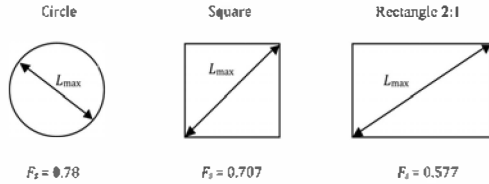


Figure 1: Illustration of calculating the shape number for a connected region

Note that the maximum value of $F_s = \frac{\pi r^2}{(2r)^2} = \frac{\pi}{4} = 0.785$, occurs for a circle. For

simplicity in the implementation L_{max} is approximated as the maximum distance between pixels in the horizontal or vertical direction, and the area is the number of pixels, N_{pixel} , that make up the shape. Therefore F_s in Equation (2) is redefined:

$$F_s = \frac{N_{pixel}}{\max[\Delta x_{pixel}, \Delta y_{pixel}]^2} \quad (3)$$

$$\Delta x_{pixel} = \max(x_{pixel}) - \min(x_{pixel}) \quad (4)$$

$$\Delta y_{pixel} = \max(y_{pixel}) - \min(y_{pixel}) \quad (5)$$

Equation (3) slightly changes F_s for the square and rectangle examples given in Moss et al [10]. The adjusted values are shown in Figure 2. The shape factors of a true and false exudate are given in Figures 3 and 4 respectively. In Figure 3 the geometry is quite close to a circle giving a relatively large value of $F_s=0.64$, where for Figure 4 the exudate is far from circular with a value of $F_s=0.18$. A threshold of 0.4 was found effective in ruling out false positives.

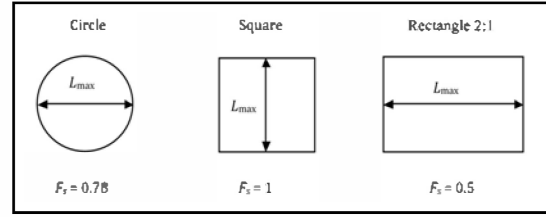


Figure 2: Simplified calculation of the shape number for a connected region.

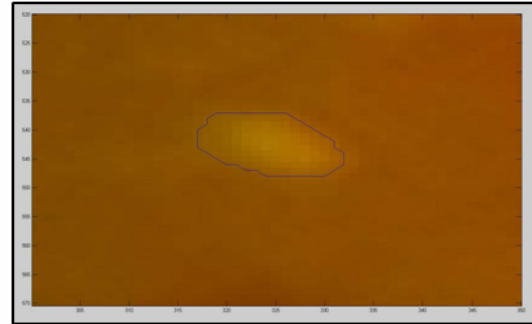


Figure 3: True exudate with area=108 and $F_s=0.64$

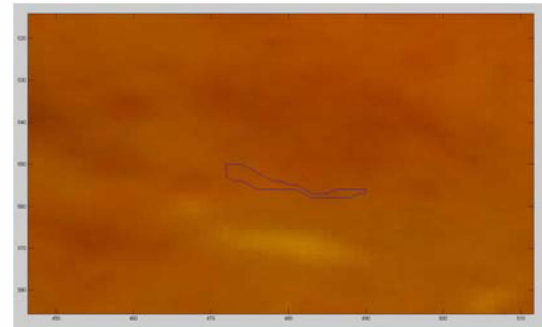


Figure 4: False exudate with area=19 and $F_s=0.18$

A summary of the area and F_s method is given in Figure 5.

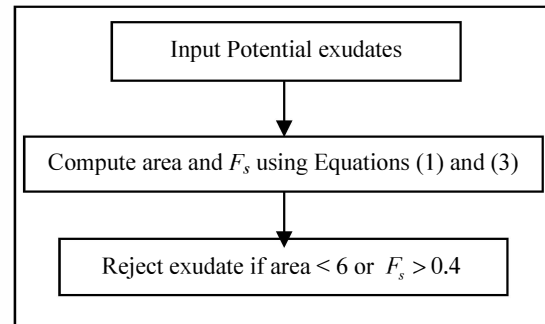


Figure 5: Summary of area and F_s algorithm

2.2.2 Closed contour

For a given potential exudate, the contours of the red/green intensity surface are computed in steps of 0.05 ± 0.5 around the mean red/green ratio of the exudates and up to 7 contours are selected as explained in Step IV of the algorithm in Section 2.1.

Figures 6 and 7 show the result for a true and false exudates respectively. One clear property that is revealed is that all the contours on the true exudates of Figure 6 are closed unlike those of Figure 7. Hence a further step in the algorithm is to determine if the first and last point of each surrounding contour coincide. If any contour fails this closure condition, the potential exudate is rejected.

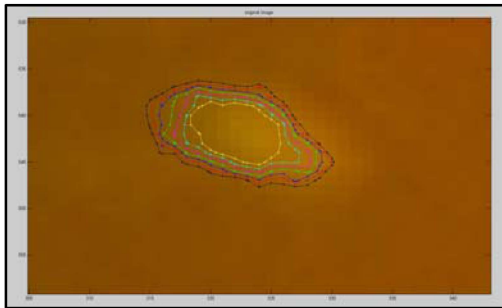


Figure 6: Closed contours surrounding a true exudate

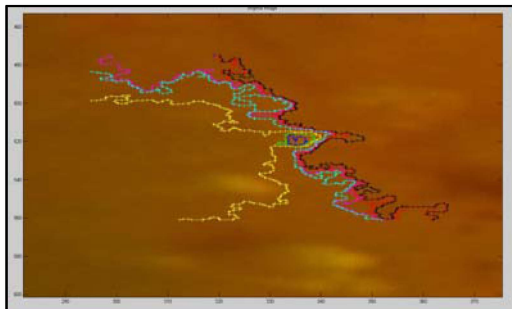


Figure 7: Open contours surrounding a false exudate

2.2.3 “Hole” measure

An exudate is a yellow dot on the retina so has very little red intensity but a significant amount of green intensity. Therefore, the red/green intensity surface corresponding to a region containing the exudate will have a hole where the red/green intensity suddenly drops. Figure 8 shows an example of this effect, where the red/green intensity drops from

approximately 2 to 1 when moving from outside to inside of an exudate.

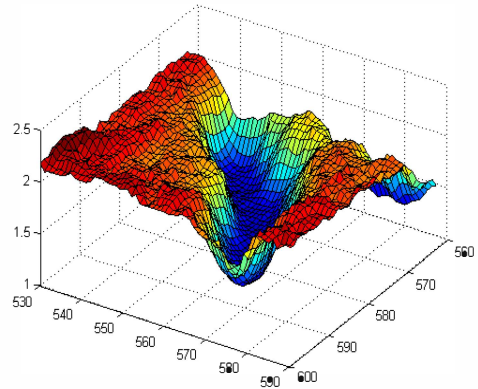


Figure 8: Example of the red/green surface in a region containing an exudate.

Hence, it is desired to develop a metric which describes this hole. To ensure that the full spatial effect is described a series of slices rotating about the centre of the exudates are performed. On the $x-y$ plane these slices correspond to lines at various angles about the exudates centre. To simplify the image processing and to speed up computation time, 4 perpendicular lines are chosen at angles from the vertical of 0, 45, 90 and 135 degrees. It is assumed that these slices are sufficient to describe the “hole”, but further work is required to fully validate whether or not the use of more lines has any effect on sensitivities or specificities the DR detection algorithm. Figure 9 shows the four lines.

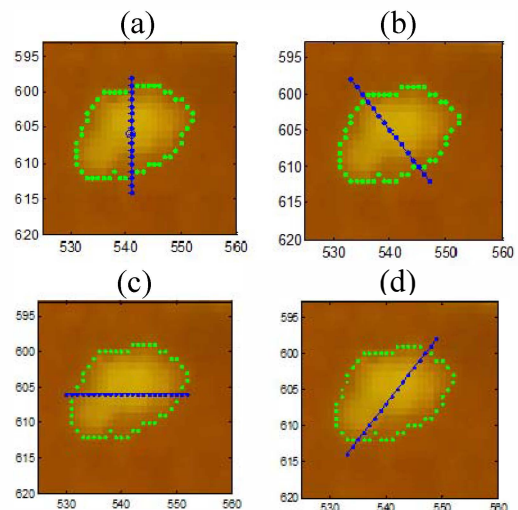


Figure 9: Four lines through the centre of an exudate corresponding to angles from the vertical of: (a) 0 degrees (b) 45 degrees (c) 90 degrees (d) 135 degrees

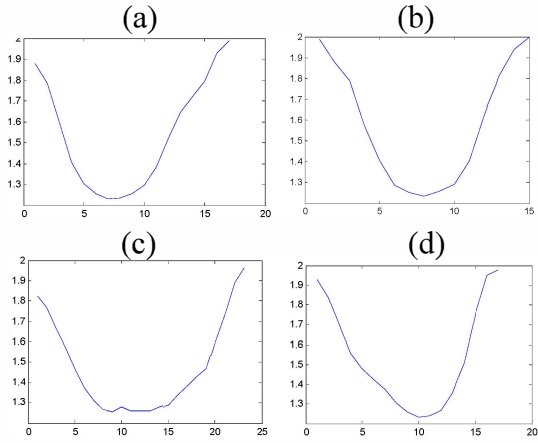


Figure 10: Red/green intensity plots for the lines through an exudate in Figure 9: (a) 0 degrees (b) 45 degrees (c) 90 degrees (d) 135 degrees

The length of each line is determined by moving 2 pixels either side of the boundary of the initially detected potential exudate. The characteristics of the red/green surface in Figure 8 are thus approximated by the geometry of the red/green intensities along each of the lines in Figures 9 (a)-(d). The corresponding intensity plots are shown in Figures 10 (a)-(d). These curves are “U” shaped and clearly reveal a “hole”. Figure 10 gives an example of a false exudate with the corresponding red/green intensities plotted in Figure 11. These curves typically slope up or down and are thus topologically quite different from those curves in Figure 9.

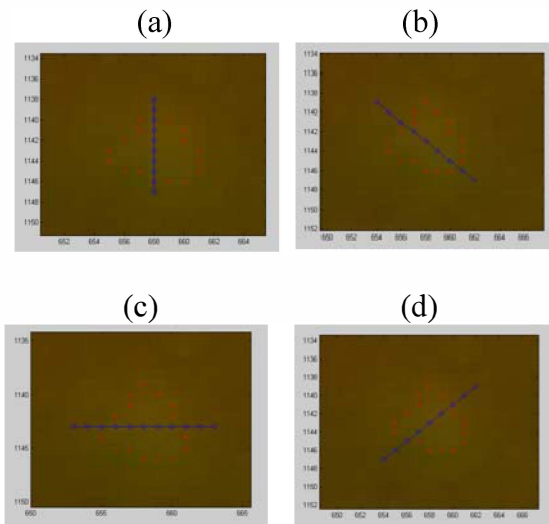


Figure 11: Four lines through the centre of a false exudate corresponding to angles from the vertical of: (a) 0 degrees (b) 45 degrees (c) 90 degrees (d) 135 degrees

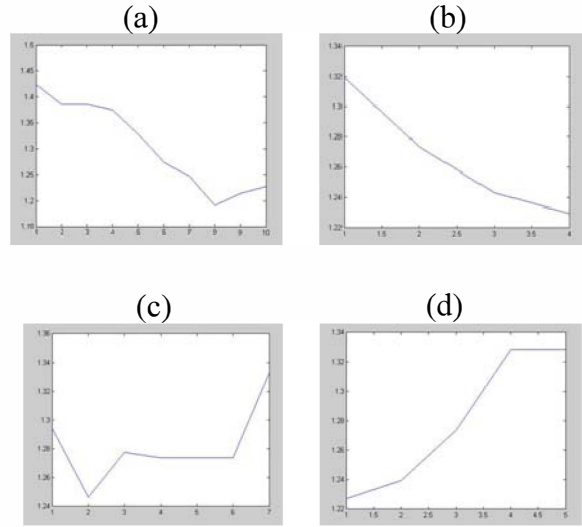


Figure 12: Red/green intensity plots for the lines through a false exudate in Figure 11: (a) 0 degrees (b) 45 degrees (c) 90 degrees (d) 135 degrees

The results of Figures 10 and 12 motivate a distance metric which is high for a deep “U” shaped curve and small for any other shaped curves. If the “U” shaped curve is deep corresponding to a bright exudate, then there will be a large difference in intensity between the minimum intensity and the intensities of both the left and right hand end points. Figure 12 (a) has a relatively large difference in intensity of 0.2 between the minimum intensity and the intensity at the left hand end point, but the difference to the right hand end point is only 0.05. For this particular exudate shown in Figure 11, the reason for the essentially monotonic decreasing or increasing R/G curves is that the exudate occurs reasonably close to a vein. As the line gets closer to the vein the red channel increases and the green channel decreases which gives an increase in R/G.

To mathematically describe this effect, first define:

$$I_{\theta, \text{left}} \equiv \text{intensity at left hand end-point} \quad (6)$$

$$I_{\theta, \text{right}} \equiv \text{intensity at right hand end-point} \quad (7)$$

$$I_{\theta, \text{min}} \equiv \text{minimum intensity} \quad (8)$$

where θ is the angle of the corresponding line through the exudate centre as shown in Figures 9 and 11. For each θ , the “hole” metric is defined:

$$\delta_{\theta} = \min \{ I_{\theta, \text{left}} - I_{\theta, \text{min}}, I_{\theta, \text{right}} - I_{\theta, \text{min}} \} \quad (9)$$

$$\delta_{\text{hole}} = \text{mean} \{ \delta_{\theta} : \theta = 0^{\circ}, 45^{\circ}, 90^{\circ}, 135^{\circ} \} \quad (10)$$

Tables 1 and 2 give the results of computing δ_θ for the exudates of Figures 9 and 11. The values of δ_θ are significantly larger by an order of magnitude for a true exudate compared to a false exudate as expected.

Table 1: Hole metric for true exudate of Figure 9

Angle (degrees)	Hole metric, δ_θ
0°	0.65
45°	0.75
90°	0.57
135°	0.69
Mean (δ_{hole})	0.67

Table 2: Hole metric for false exudate of Figure 11

Angle (degrees)	Hole metric, δ_θ
0°	0.03
45°	0.04
90°	0.08
135°	0.05
Mean (δ_{hole})	0.06

2.3 Summary of overall algorithm

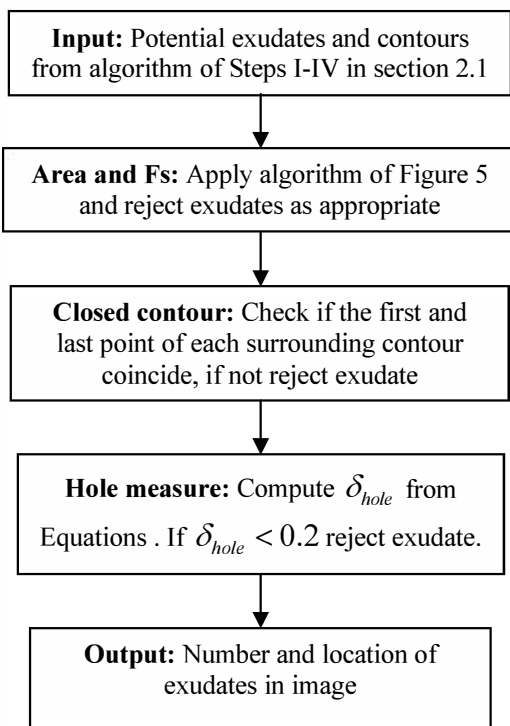


Figure 13: Overall algorithm for selecting exudates

3 Results and Discussion

The main purpose of this paper is to check the effectiveness of new geometric measures to rule out or accept potential exudates that are found using an initial pre-screening method. This initial step uses more traditional approaches to detect DR using a median filter (see e.g. [ref]). The geometric measures can be used to better describe and model with understanding and clarity, the underlying physiology, in contrast to the usual neural network or classifier approach that has not yet proven effective [ref].

Hence the specificities are calculated with respect to the number of potential exudates from the initial screening method that are false. The sensitivities on the other hand are calculated by manually counting the number of true exudates in each image. Unfortunately, the image set used in this research does not have fully graded individual DR. The grading is only in terms of the presence or absence of DR. Hence, since no qualified ophthalmologist graded the individual exudates of the images used in this paper, the results can only be considered as preliminary and a basic proof of concept.

The algorithm of Figure -- was tuned on several darker images, the same as were chosen to find the thresholds in [ref]. The methods were initially tested on 6 new images including one clean image, for verifying the accuracy. The individual results are shown in Table 3 where the typical diagnostic measures of specificity, sensitivity, positive predictive value (PPV) and negative predictive value (NPV) are used.

Very high specificities can be observed in each case, showing that the algorithm of Figure – is very effective at ruling out false exudates. The percentage sensitivities are also in general high, with the exception of images 4 and 5 where the values are 75% in each case. There were very few true exudates in these cases and the false negatives were very small and ruled out due to an area < 6 pixels. This area could potentially be reduced to avoid these false negatives, but would require a re-working of the contour method and hole measure as a separate special case. However, there is also some doubt on whether these very small exudates are indeed exudates.

A further six arbitrarily chosen images were then tested including 2 clean images to give a total of 12 images in the testing set. The overall results are given in Table 4 which again show very high specificities and good sensitivities.

Table 3: Individual sensitivity and specificity of algorithm for initial 6 images

Image 1	M1	M0	
	M1	3	0
	M0	0	6
	Sensitivity	100.0	Specificity 100.0
Image 2	M1	M0	
	M1	19	0
	M0	1	9
	Sensitivity	95.0	Specificity 100.0
Image 3	M1	M0	
	M1	3	0
	M0	1	16
	Sensitivity	75.0	Specificity 100.0
Image 4	M1	M0	
	M1	6	0
	M0	2	1
	Sensitivity	75.0	Specificity 100.0
Image 5	M1	M0	
	M1	125	1
	M0	18	10
	Sensitivity	87.4	Specificity 90.9
Image 6	M1	M0	
	M1	0	0
	M0	0	46
	Sensitivity	100.0	Specificity 100.0

Table 4: Overall sensitivity and specificity for initial 6 images plus another 6 new images

Image 1	M1	M0	
	M1	281	3
	M0	36	184
	Sensitivity	88.6	Specificity 98.4

The results from the 12 images demonstrate that high sensitivities can be obtained without dramatically reducing the specificity which is usually the case in the literature. A further result, is that in terms of detecting the presence or absence of exudates, the algorithm performed with 100% specificity and 100% sensitivity. A similar successful result was found in

[9]. Adjusting the thresholds have also been shown to lift the sensitivity to above 90% while maintaining specificity above 95%. This result is not surprising and many diagnostic methods actually choose thresholds to optimize sensitivity. This approach could be easily included in the current algorithm as required.

Hence the mathematical and geometrical methods developed in [9] and this paper have the potential for assisting in the screening of DR and justify the future involvement of ophthalmologists which is planned.

4 Future planned work with ophthalmologists

The algorithms developed in this paper and [9] can provide the tools to tackle any form of DR. The concept is to relate physiological aspects, like the yellow color of exudates to geometrical properties that can be described mathematically. A very important aspect of computer based algorithms that this research and most typical approaches do not address is the use or integration of an ophthalmologist's technique of diagnosing DR. Eye tracking has been commonly used to characterize a good radiologist and has been used for training aspects as well. Future work in collaboration with the Christchurch Van der Veer Institute will analyse what parts of the retina experienced ophthalmologists focus on and what time they spend in the various regions.

In the current research of this paper and [9], it has been found that exudates commonly circle the fovea. The fovea is the absolute centre of vision so cones and rods in the eye are more dense in this region. Hence future work will look at how they distribute, what physiological mechanisms are involved and how this information can be used in the methods. Importantly, it would be very interesting if ophthalmologists naturally looked in this region too and would thus form an initial hypothesis for testing during the planned eye tracking study. Hence the idea is to take aspects of the ophthalmologist's experience as well as physiology, and put into the algorithms.

Some initial tests have been performed at the Christchurch Van der Veer Institute on healthy subjects, to test the accuracy and feasibility of the proposed study. Figure 14 shows an example of tracking the eye along a vein, with an initial starting sequence of the optic disk, fovea, optic disk. The size of the circle is proportional to the amount of time spent at that particular region. Many other statistics that summarize common aspects amongst groups of people, are automatically available on the system. For example, the spatial distribution on the key regions of the retina where the "average" ophthalmologists

focuses can be characterized. Thus, the planned study which would involve eye-tracking of 5-10 ophthalmologists, is quite feasible and the system has a sufficiently accurate resolution.

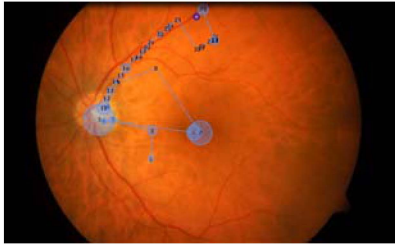


Figure 14: An example of eye tracking along a vein

5 Conclusion

A set of geometrical methods for ruling out false exudates from an initial screening method based on the median filter [9] were developed. A major part of these methods was the use of contours of the red/green intensities that surround true exudates. For false exudates a simple check of the closure of the contours ruled out a large number of false exudates. This check was followed by a hole measure which accounts for 3D spatial information surrounding the exudates. These analytical techniques were shown to give very high specificities with up to 12 images tested. This result shows that the algorithm correctly rejects false exudates in the majority of cases, which is what the algorithm was primarily designed for. Equally importantly, sensitivities still remained high around ~90%. These sensitivities could be further increased as required with a corresponding approximately equal drop in specificities which are currently around 98%.

References

- [1] A. Icks, C. Trautner, B. Haastert, M. Berger, and G. Giani. "Blindness due to diabetes: population based age- and sex- specific incidence rates," *Diabet Med.*, vol. 7, pp. 571-575, 1997.
- [2] D. Fong, L. Aiello, T. Gardner, G. King, G. Blankenship, J. Cavallerano, F. Ferris and R. Klein. "Retinopathy in Diabetes," *Diabetes Care*, vol 27, pp. 584-587, 2004.
- [3] R. J. Tapp, J. E. Shaw, C. A. Harper, et al. "The prevalence of and factors associated with diabetic retinopathy in the Australian population," *Diabetes Care*, vol 26(6), pp. 1731-1737, 2003.
- [4] J. H. Kempen, B. J. O'Colmain, M. C. Leske, S. M. Haffner, R. Klein, S. E. Moss, H. R. Taylor, R. F. Hamman. "Eye Diseases Prevalence Research Group. The prevalence of diabetic retinopathy among adults in the United States," *Arch Ophthalmol.*, vol 122(4), pp. 552-563, 2004.
- [5] D.S. Fong, L.L. Aiello, T.W. Gardner, G.L. King, G. Blankenship, J. D. Cavallerano, F. L. Ferris, and R. Klein. "Retinopathy in Diabetes," *Diabetes Care*, vol 27, 2004.
- [6] P.J. Kertes, T.M. Johnson, editors. Evidence based eye care. Lippincott Williams & Wilkins, 2007.
- [7] S. Wild, G. Roglic, A. Green, R. Sicree, H. King. "Global prevalence of diabetes: estimates for the year 2000 and projections for 2030," *Diabetes Care*, vol 27(5), pp. 1047-1053.
- [8] M.D. Abramoff, M. Niemeijer, M.S. Suttorp-Schulten, M. A. Viergever, S.R. Russell, B. Van Ginneken. "Evaluation of a system for automatic detection of diabetic retinopathy from color fundus photographs in a large population of patients with diabetes," *Diabetes Care*, vol 31(2), pp.193-198, 2008.
- [9] C.E. Hann, D. Hewett, J.A. Revie, J.G. Chase and G.M. Shaw. "Screening for Diabetic Retinopathy Using Computer Vision and Physiological Markers," *Journal of Diabetes Science and Technology (JoDST)*, vol 3(4), pp. 819-834, 2009.
- [10] S.E. Moss, R. Klein, S.D. Kessler, K.A. Richie. "Comparison between ophthalmoscopy and fundus photography in determining severity of diabetic retinopathy," *Ophthalmology*, vol 92(1), pp.62-67, 1985.